Inorganic Chemistry

Article

pubs.acs.org/IC

Hydrogen in $La_2MgNi_9D_{13}$: The Role of Magnesium

Roman V. Denys,[†,‡] Volodymyr A. Yartys,*[,†,§] and Colin J. Webb[∥]

[†]Institute for Energy Technology, P.O. Box 40, Kjeller, NO 2027, Norway

[‡]Karpenko Physico-Mechanical Institute of NAS of Ukraine, Lviv 79601, Ukraine

[§]Norwegian University of Science and Technology, Trondheim NO 7491, Norway

[∥]Griffith University, Kessels Road, Nathan 4111, Brisbane, Australia

Supporting Information

ABSTRACT: Reversible hydrogen storage capacity of the $La_{3-x}Mg_xNi_9$ alloys, charged by gaseous hydrogen or by electrochemical methods, reaches its maximum at composition La_2MgNi_9. As $(La,Mg)Ni_{3-3.5}$ alloys are the materials used in advanced metal hydride electrodes in Ni−MH batteries, this raises interest in the study of the structure−properties interrelation in the system La_2MgNi_9−H_2 (D_2). In the present work, this system has been investigated by use of *in situ* synchrotron X-ray and neutron powder diffraction in H_2/D_2 gas and by performing pressure−composition−temperature measurements. The saturated $La_2MgNi_9D_{13.1}$ hydride forms via an isotropic expansion and crystallizes with a trigonal unit cell (space group $R\bar{3}m$ (No.166); a = 5.4151(1) Å; c = 26.584(2) Å; V = 675.10(6) Å^3). The studied hybrid structure is composed of a stacking of two layers resembling existing intermetallic compounds $LaNi_5$ ($CaCu_5$ type) and $LaMgNi_4$ (Laves type). These are occupied by D to form $LaNi_5D_{5.2}$ and $LaMgNi_4D_{7.9}$. The $LaNi_5D_{5.2}$ slab has a typical structure observed for all reported $LaNi_5$-containing hybrid structures of the AB_5 + Laves phase types. However, the Laves type slab $LaMgNi_4D_{7.9}$ is different from the characterized individual $LaMgNi_4D_{4.85}$ hydride. This results from the filling of a greater variety of interstitial sites in the $La_2MgNi_9D_{13}$/$LaMgNi_4D_{7.9}$, including $MgNi_2$, Ni_4, $(La/Mg)_2Ni_2$, and $(La/Mg)Ni_3$, in contrast with individual $LaMgNi_4D_{4.85}$ where only La_2MgNi_2 and Ni_4 interstitials are occupied. Despite a random distribution of La and Mg in the structure, a local hydrogen ordering takes place with H atoms favoring occupation of two Mg-surrounded sites, triangles $MgNi_2$ and tetrahedra $LaMgNi_2$. A directional bonding between Ni, Mg, and hydrogen is observed and is manifested by a formation of the NiH_4 tetrahedra and MgH_6 octahedra, which are connected to each other by sharing H vertexes to form a spatial framework.

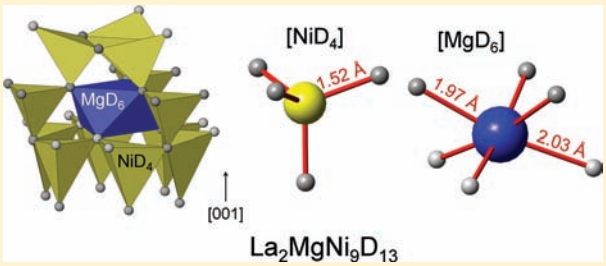

INTRODUCTION

Ternary La−Mg−Ni hydrogen storage alloys with composition $La_{1-x}Mg_xNi_y$ (x = 0.2−0.4, y = 3−4) attract significant interest as materials for the negative electrodes in Ni−metal hydride (MH) batteries. The electrochemical discharge capacity of such alloys reaches 400 mAh/g which is 25% greater than that of the commercial AB_5-type based electrodes, 315 mAh/g.[1,2]

The most important series of these alloys for hydrogen storage/electrochemical applications include $La_{3-x}Mg_xNi_9$, $La_{4-x}Mg_xNi_{14}$, and $La_{5-x}Mg_xNi_{19}$ crystallizing with, respectively, trigonal $PuNi_3$, hexagonal Ce_2Ni_7, hexagonal Pr_5Co_{19}, or trigonal Ce_5Co_{19} types of crystal structures.[3−5] All these alloys belong to a family of hybrid layered structures, where a single Laves type $La_{2-x}Mg_xNi_4$ layer and several Haucke ($CaCu_5$) type $LaNi_5$ layers stack along the hexagonal/trigonal axes.

Despite extensive studies of the electrochemical properties of La−Mg−Ni alloys over the past years, no systematic studies have been performed on the structure of the corresponding hydrides and influence of Mg→La substitution on their structural and hydrogenation behaviors.

In an earlier publication, we reported on $La_3MgNi_{14}D_{18.2}$ deuteride formed by the Ce_2Ni_7-type intermetallic alloy and probed by neutron powder diffraction.[6] The study showed that magnesium has a significant effect on the hydrogenation behavior, and that (a) instead of a strong unidirectional anisotropic expansion which takes place on hydrogenation of La_2Ni_7,[7] for La_3MgNi_{14} an isotropic hydrogen-induced expansion proceeds in the basal plane and along [001] direction, (b) in contrast to $La_2Ni_7D_{6.5}$ where only $LaNi_2$ layers accommodate hydrogen atoms, in $La_3MgNi_{14}D_{18.2}$ both $LaNi_5$ and $LaMgNi_4$ layers become occupied by D, and (c) the metal matrix is not affected by amorphization and disproportionation on cycling of hydrogenation−decomposition because of the stabilization of the metal sublattice by Mg. In a recent study of $La_4MgNi_{19}D_{21.8}$ deuteride,[8] hydrogen atoms were similarly found to be evenly distributed over the $LaNi_5$ and $LaMgNi_4$ layers, with nine types of interstitial sites filled and a rather even expansion of these two slabs.

In a recent publication we presented general thermodynamic and structural studies of the $La_{3-x}Mg_xNi_9$-based hydrides.[9] Magnesium influences structural features of the hydrogenation

Received: December 15, 2011
Published: March 14, 2012

   dx.doi.org/10.1021/ic202705u | Inorg. Chem. 2012, 51, 4231−4238

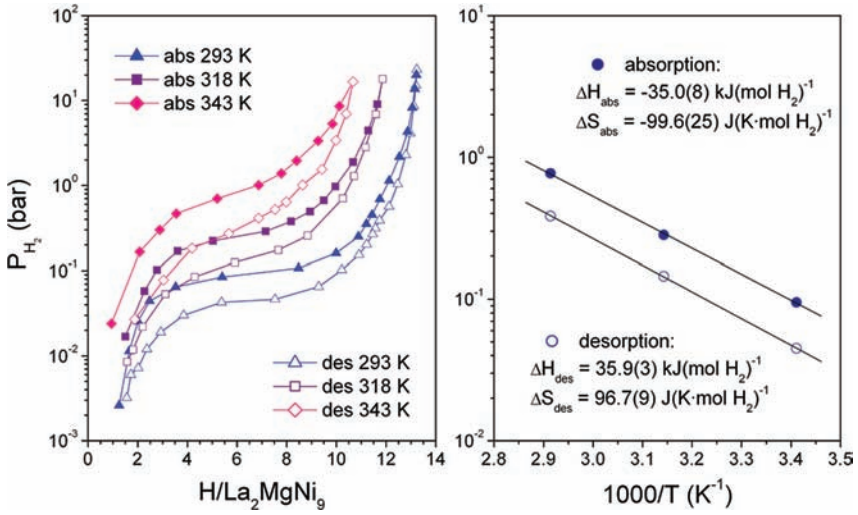

Figure 1. PCT diagrams for the system La_2MgNi_9–H_2: (a) hydrogen absorption–desorption isotherms and (b) van't Hoff plots.

process and determines various aspects of the hydrogen interaction with the $La_{3-x}Mg_xNi_9$ intermetallics causing (a) more than 1000 times increase in equilibrium pressure of hydrogen absorption and desorption for the Mg-rich $LaMg_2Ni_9$ as compared to the Mg-poor $La_{2.3}Mg_{0.7}Ni_9$ and a substantial modification of the thermodynamics of the formation–decomposition of the hydrides, (b) an increase in reversible hydrogen storage capacities following an increase in Mg content in the $La_{3-x}Mg_xNi_9$ to ~1.5 wt % H for La_2MgNi_9, (c) improvement of resistance against hydrogen-induced amorphization and disproportionation, and (d) change of the mechanism of the hydrogenation from anisotropic to isotropic.

The present work is focused on a detailed study of the hydrogenation properties and crystal structure of the $La_2MgNi_9(H,D)_{13}$ hydride. La_2MgNi_9 composition has been chosen because it has the highest gravimetric and electrochemical charge–discharge capacity among the $La_{3-x}Mg_xNi_9$ (x = 0–2) alloys.[9,10]

EXPERIMENTAL SECTION

La_2MgNi_9 alloy was prepared by a powder metallurgy synthesis route from the $LaNi_{4.5}$ alloy precursor and Mg powder (Alfa Aesar, 325 mesh, 99.8%). The $LaNi_{4.5}$ alloy was arc melted from the individual metals, La (99.98%) and Ni (99.9%), in a protective atmosphere of purified argon gas. As cast alloy was crushed into powder and mixed with magnesium in an argon atmosphere. The powder mixture (m = 5 g) was ball milled in a SPEX 8000D mill under argon for 8 h using a ball to powder ratio of 4:1. After the milling process, the mixture was annealed in an argon atmosphere and then quenched to room temperature. The annealing was performed in two steps: first at 1073 K for 8 h, followed by a second step at 873 K for 8 h. A small excess of Mg was introduced into the initial mixture to compensate for its evaporation at high temperatures.

The characterization of the alloy was performed using synchrotron X-ray diffraction (SR XRD). High-resolution SR XRD data were collected at the Swiss-Norwegian Beamlines (SNBL, BM01B) at ESRF, Grenoble, France. A monochromatic beam with λ = 0.5014(1) Å was provided by a double Si monochromator. A 2θ angular range of 1–50.5° was scanned with a detector bank consisting of six scintillation detectors mounted in series with 1.1° separation. The data was binned to the step size $\Delta 2\theta$ = 0.003°. The instrumental contribution to the line broadening was evaluated by refining the profile parameters for a standard Si sample. The experimental SR XRD data were refined with the Rietveld method using the Fullprof program.[11] SR XRD patterns are shown in Figure S1 (Supporting Information). Refinements showed that the vast majority of the sample was composed of $La_{2.0}Mg_{1.0}Ni_9$ intermetallic with $PuNi_3$ type of structure (space group $R\bar{3}m$ (No.166); a = 5.0314(2) Å, c = 24.302(1) Å). In addition, a small amount of $LaMgNi_4$ ($MgCu_4Sn$ type; space group $F\bar{4}3m$ (No. 216), a = 7.1694(7) Å), 6.8(3) wt %, was identified as an impurity phase. In the structure of La_2MgNi_9, Mg substitution proceeds exclusively on the 6c site in the Laves type layer and reaches 50%, whereas the 3a site remains occupied by La atoms only. Structural parameters for the La_2MgNi_9 compound (see Table S1 in Supporting Information) are in good agreement with literature data.[10]

Hydrogen absorption–desorption behavior of the La_2MgNi_9 alloy was characterized using the Sieverts' type technique. The sample was activated in vacuum at 573 K for 30 min, cooled to 293 K, and then charged with high purity hydrogen gas (99.999% H_2). Pressure–composition–temperature (PCT) dependences of hydrogen absorption and desorption were measured at temperatures of 293, 318, and 343 K using hydrogen pressures from 0.001 to 25 bar. Several complete hydrogen absorption–desorption cycles were performed prior to the PCT measurements in order to improve the kinetics of hydrogen exchange and to achieve maximum hydrogen storage capacities.

In situ SR XRD studies were performed at beam station BM1B of the Swiss-Norwegian Beamlines, ESRF, Grenoble, France, using a monochromatic X-ray beam with λ = 0.5014(1) Å. A small amount of the alloy powder was loaded into an open-ended 0.3 mm quartz capillary, which was then placed inside a sealed 0.5 mm quartz capillary connected to the Sieverts' type gas system via a modified Swagelok-Tee joint attached to a goniometer head. The inner open-ended capillary was used to prevent breakage of the sample cell capillary from the stresses created by hydrogenation-induced expansion of the alloy. Averaging over the different orientations of the crystallites, resulting in the elimination of the preferred orientation effects in the collected diffraction data, was achieved by oscillating the sample cell around the axis of the capillary. Heating and cooling of the sample was performed at constant rates by a programmable Cyberstar gas blower. A turbomolecular vacuum pump provided the vacuum. First, the sample was activated in vacuum at 623 K for 30 min. Then the sample was cooled, and on reaching 363 K, the high purity hydrogen gas (99.999% H_2) at pressure of 10 bar was introduced into the sample capillary. After that the capillary was slowly cooled to room temperature at a constant cooling rate of 1.5 K/min. At the applied pressure a complete transformation into the hydride was observed in a temperature range from 348 to 328 K. The diffraction data (2θ range 10–16.7°; step size $\Delta 2\theta$ = 0.006°) were collected every 40 s. Finally, for accurate structural characterization of the saturated hydride, room temperature SR XRD diffraction data were collected at a 2θ angular range 1–50.5° with a step size $\Delta 2\theta$ = 0.004°.

dx.doi.org/10.1021/ic202705u | *Inorg. Chem.* 2012, 51, 4231–4238

In situ neutron powder diffraction (NPD) studies of the $La_2MgNi_9D_{13}$ deuteride were performed at the Spallation Neutron Source SINQ accommodated at Paul Scherrer Institute, Villigen, Switzerland, using the high resolution powder diffractometer HRPT in the high intensity mode (λ = 1.494 Å, 2θ range 4.05−164.9°, step size 0.05°). The deuteride was synthesized in a stainless steel container (wall thickness 0.2 mm, d_{inner} = 6 mm), which was connected to a Sieverts' type apparatus and used as the sample cell during the *in situ* NPD experiment. The initial alloy sample was activated in vacuum at 573 K and charged by deuterium gas (99.8% purity) at room temperature and pressure of 10.2 bar. The neutron diffraction data obtained were refined with the Rietveld method using the GSAS software.[12]

RESULTS

Hydrogen Storage Capacity and Thermodynamic Stability of the Hydride. The activated La_2MgNi_9 alloy showed rather fast hydrogen absorption kinetics from the first hydrogenation at 293 K under 10 bar H_2, reaching capacity of 13 at. H/La_2MgNi_9 in less than 10 min. The composition of the saturated hydride was determined to be $La_2MgNi_9H_{13}$, and this slightly increased to $La_2MgNi_9H_{13.3}$ following a pressure increase from 10 to 23 bar H_2.

Hydrogen absorption−desorption isotherms of the La_2MgNi_9−H_2 system are presented in Figure 1. The studied system shows single plateau behavior of a transformation from α-solid solution of hydrogen in the intermetallic alloy to a corresponding β-hydride phase. At room temperature, the plateaux are located at 0.1 bar H_2 for H-absorption and 0.05 bar H_2 for the desorption, thus showing quite a significant hysteresis between these two processes, P_{abs}/P_{des} = 2.0. However, despite the hysteresis, the values of the equilibrium pressures nicely suit the purpose of electrochemical charge−discharge of the alloy by hydrogen. Thus, both the kinetics of hydrogen exchange and the thermodynamics of the metal−hydrogen interactions allow applications of the alloy as a battery electrode material in nickel metal hydride batteries.

La_2MgNi_9 has a slightly higher hydrogen storage capacity of 1.09 H/M (hydrogen atoms per metal atom) compared to the other characterized representatives of the hybrid La−Mg−Ni compounds, La_3MgNi_{14}[6] and La_4MgNi_{19}[8] (respectively, 1.03 and 0.91 H/M). From the PCT measurements it is clear that La_2MgNi_9-based hydride is the most stable of the three mentioned hydrogenated alloys (with enthalpy of hydrogen desorption being 35.9 kJ/mol H_2, as compared to the values of 33.6 kJ/mol H_2 for La_3MgNi_{14}[6] and 31.5 kJ/mol H_2 for La_4MgNi_{19}[5]). The reversible hydrogen storage capacity of La_2MgNi_9 at room temperature reaches 1.5 wt % H, which corresponds to an electrochemical capacity of 400 mAh/g.

***In situ* SR XRD Study of Hydrogen Absorption by La_2MgNi_9.** Figure 2 shows the evolution of the SR XRD pattern during cooling of the La_2MgNi_9 alloy from 363 K to room temperature at a rate of 1.5 K/min under a hydrogen pressure of 10 bar. A solid solution of hydrogen in the intermetallic alloy, α-$La_2MgNi_9H_x$, starts to form immediately after hydrogen is introduced into the sample cell. This leads to the peaks broadening and their slight shift toward the lower diffraction angles indicating a lattice expansion. Below 350 K the intermetallic alloy transforms into the β-hydride; the latter transformation is identified from the appearance of new diffraction lines, which can be indexed in the same trigonal symmetry as for the initial alloy, although with a significant expansion of the unit cell, $\Delta V/V \approx 26\%$. A two-phase region of coexistence of the α-solid solution and β-hydride phase is

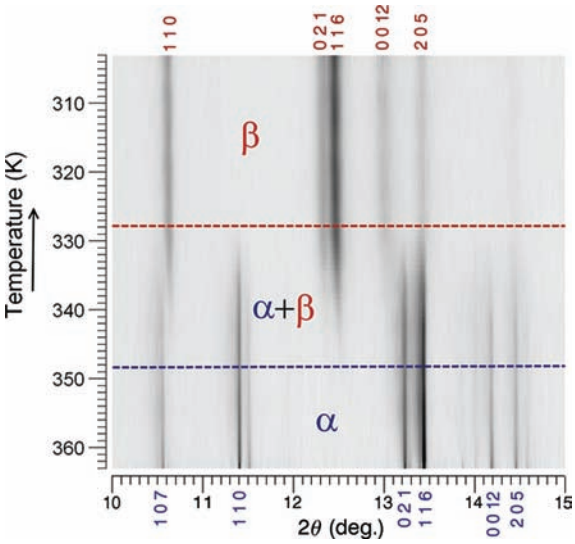

Figure 2. *In situ* SR XRD pattern (BM01B; λ = 0.5014(1) Å) of hydrogen absorption in the La_2MgNi_9−H_2 system during cooling of the sample at a constant H_2 pressure of 10 bar (cooling rate of 1.5 K/min). Miller indexes (space group $R\bar{3}m$ of the strongest reflections from α-$La_2MgNi_9H_x$ and β-$La_2MgNi_9H_{\sim 13}$ are shown at the bottom and top of the figure, respectively.

observed from 348 to 328 K. At 328 K the transformation into the hydride phase was complete. Observation of a two phase region during the *in situ* SR XRD study is in full agreement with the PCT measurements, showing single plateau equilibrium between the α- and β-phases.

A high-resolution SR XRD pattern from the saturated $La_2MgNi_9H_{13}$ hydride measured at room temperature and 10 bar H_2 is given in Figure S2 (Supporting Information). Rietveld refinements confirmed that the trigonal symmetry of metal matrix is retained after hydrogenation (space group $R\bar{3}m$ (No.166); a = 5.4127(8) Å, c = 26.597(5) Å). The detailed structural data for $La_2MgNi_9H_{13}$ is given in Table S1 (Supporting Information). Hydride formation is accompanied by isotropic expansion of the unit cell, $\Delta a/a$ = 7.6%, $\Delta c/c$ = 9.4% ($\Delta V/V$ = 26.7%). We note that almost equal volume expansion of Laves and $CaCu_5$ type slabs occurs during formation of $La_2MgNi_9H_{13}$, namely 27.1% and 26.2%, respectively. This observation assumes even distribution of H atoms in the structure of the hydride. The structural model of the metal matrix obtained from SR XRD data has been used as a starting point in the refinement of the neutron diffraction data.

Crystal Structure of $La_2MgNi_9D_{13}$. The same pressure−temperature conditions (10 bar D_2 and room temperature) were used for the collection of both *in situ* SR XRD and *in situ* NPD data for the studied deuteride $La_2MgNi_9D_{13}$. The starting model for the structure of $La_2MgNi_9D_{13}$ was based on the atomic structure of the metal sublattice derived from the synchrotron XRD data. On the basis of this data, we have accomplished crystallographic analysis of the sizes and surrounding of all potentially available deuterium interstitial positions in the metal matrix and have considered possible models of the D sublattice. The D atoms were localized from the difference nuclear density maps (Fourier analysis). Eight D sites were selected and introduced into the NPD Rietveld refinements. In total, there were 17 independent positional parameters refined (4 for metal and 13 for the D atoms), as

dx.doi.org/10.1021/ic202705u | *Inorg. Chem.* 2012, 51, 4231−4238

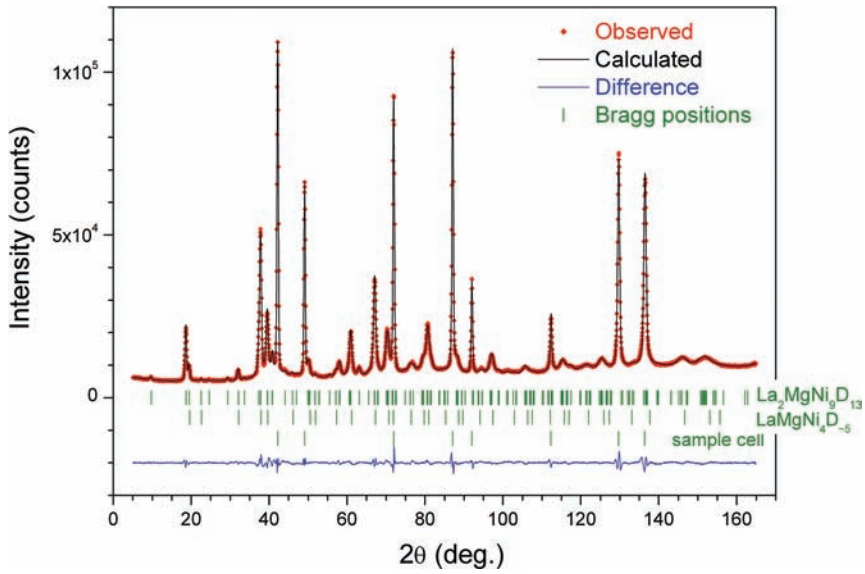

Figure 3. *In situ* powder neutron diffraction pattern of the $La_2MgNi_9D_{13}$ deuteride (300 K; 10 bar D_2). Vertical bars show positions of the Bragg peaks for the phase constituents: $La_2MgNi_9D_{13}$ (95.2 wt.%), γ-$LaMgNi_4D_{\sim 5}$ (4.8 wt %; space group $F\bar{4}3m$, a = 7.643 Å), and a stainless steel sample cell (space group $Fm\bar{3}m$; a = 3.599 Å).

Table 1. Crystal Structure Data for $La_2Mg_1Ni_9D_{13}$ from Rietveld Refinements of *in Situ* NPD Data[a]

atom	Wyckoff site	x/a	y/b	z/c	$U_{iso} \times 100$ (Å^2)	occupancy
La1	3*a*	0	0	0	3.4(2)	1.0(−)
La2/Mg	6*c*	0	0	0.1468(4)	3.7(2)	0.5/0.5(−)
Ni1	3*b*	0	0	1/2	2.2(2)	1.0(−)
Ni2	6*c*	0	0	0.3306(3)	2.1(2)	1.0(−)
Ni3	18*h*	0.4967(4)	−*x*	0.0832(1)	1.34(4)	1.0(−)
D1	18*h*	0.494(2)	−*x*	0.0196(4)	1.99(8)	0.395(6)
D2	6*c*	0	0	0.390(1)	= U_{iso}(D1)	0.28(1)
D3	18*h*	0.145(4)	−*x*	0.084(1)	= U_{iso}(D1)	0.17(1)
D4	18*h*	0.854(1)	−*x*	0.0843(4)	= U_{iso}(D1)	0.584(8)
D5	18*h*	0.4868(9)	−*x*	0.1485(3)	= U_{iso}(D1)	0.499(5)
D6	18*h*	0.798(2)	−*x*	0.1191(8)	= U_{iso}(D1)	0.25(1)
D7	6*c*	0	0	0.235(4)	= U_{iso}(D1)	0.12(1)
D8	6*c*	0	0	0.4429(5)	= U_{iso}(D1)	0.45(2)

[a]Data collected at 300 K, 10 bar D_2. Space group $R\bar{3}m$ (No. 166); a = 5.4151(1) Å, c = 26.584(2) Å, V = 675.10(6) Å^3. $\Delta a/a$ = 7.6%, $\Delta c/c$ = 9.4%, $\Delta V/V$ = 26.7%; ΔV_{LaNi_5} = 26.9%, ΔV_{LaMgNi_4} = 26.6%. Calcd D content: 13.1(3) D/f.u. (volumetric data 12.95(8) D/f.u.). *R*-factors: R_p = 2.5%; R_{wp} = 3.3%; R_{F^2} = 1.8%; χ^2 = 9.3.

well as 6 atomic displacement parameters (5 independent for the metal atoms and one common for the D atoms) and 8 site occupancy factors for each D site. For the D atoms atomic displacement parameters, U_{iso}, were constrained to be equal to avoid correlations between the occupancies of the D sites and the displacement parameters. The contribution from the secondary γ-$LaMgNi_4D_{\sim 5}$ (~5 wt %) phase and from the sample cell to the diffraction pattern was accounted by refining their scale factors only. The crystal structure data for γ-$LaMgNi_4D_{\sim 5}$ were taken from ref 15.

Refinements of the NPD data showed excellent agreement between the Rietveld profile plots of the observed and calculated NPD pattern (see Figure 3) with R_p = 2.5%, R_{wp} = 3.3%, R_{F^2} = 1.8%, χ^2 = 9.3 and yielded the following unit cell parameters of $La_2MgNi_9D_{13}$: a = 5.4151(1) Å, c = 26.584(2) Å. The crystal structure data for $La_2MgNi_9D_{13}$ is given in Table 1. As expected, the structures of the metal sublattices from SR XRD (Table S1 in Supporting Information) and from NPD data (Table 1) converge within accuracy of the refined atomic parameters.

All eight sites occupied by D appear to be partially filled with occupancies ranging from 0.12 to 0.58. The refined value of U_{iso}, 0.02 Å^2, has a typical value for D atoms in the structures of metal hydrides. Relatively large U_{iso} parameters are observed for the metal atoms, and these can result from the partial and statistical occupancies of the D sites. Depending on the occupancy or vacancy of these sites, the metal atoms in their nearest surrounding may be significantly displaced from their average crystallographic positions, yielding these observed large U_{iso} values.

In the crystal structure of $La_2MgNi_9D_{13}$, D atoms occupy both Laves and $CaCu_5$-type slabs (see Figure 4). Four D-sites are located within the $LaMgNi_4$ slab: two within the $LaNi_5$ slabs and two La(La/Mg)Ni_2 sites are placed at a boundary between the $LaMgNi_4$ and $LaNi_5$ slabs. This boundary is defined by a z position of the Ni3 atoms (z = 0.083) which form 6363 kagome nets. As both D3 and D4 are located exactly at the interslab

dx.doi.org/10.1021/ic202705u | *Inorg. Chem.* 2012, 51, 4231−4238

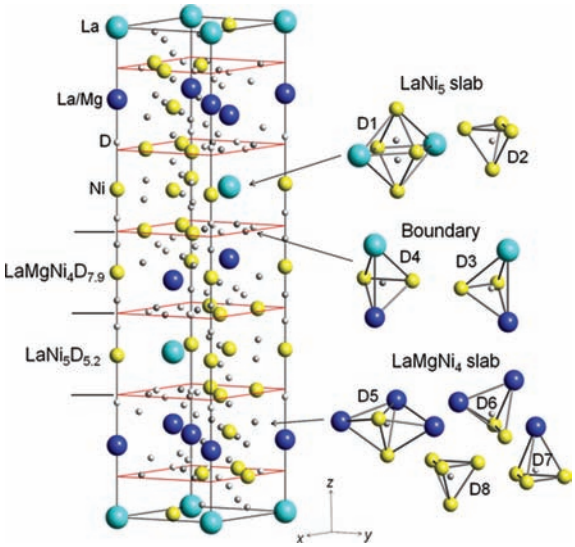

Figure 4. Crystal structure of $La_2MgNi_9D_{13.1(3)}$ showing the stacking of the $LaNi_5D_{5.2(1)}$ ($CaCu_5$ type) and $LaMgNi_4D_{7.9(2)}$ (Laves type) slabs. From 8 sites filled by D, 2 are located inside the $LaNi_5$ layer, 4 inside the $LaMgNi_4$ layer, and 2 on the border between the two slabs.

boundary (z = 0.084), they are equally related to both $LaMgNi_4$ and $LaNi_5$ slabs. From the overall stoichiometry of 13.1(3) at. D/f.u. La_2MgNi_9, 5.2(1) at. D are located in the $LaNi_5$ slabs and 7.9(2) at. D/f. u. in the $LaMgNi_4$ slabs. The calculated D content $La_2MgNi_9D_{13.1(3)}$ ($LaNi_5D_{5.2(1)}$ + $LaMgNi_4D_{7.9(2)}$) agrees within uncertainty with the value of 12.95(8) D/f.u. from the volumetric measurements during synthesis of the deuteride.

DISCUSSION

Despite quite a large volume expansion taking place during the formation of $La_2MgNi_9D_{13}$, which exceeds 25%, the relative positions of the metal atoms in the lattice remain almost unchanged. This contrasts strikingly with the hydrogenation behavior of the Mg-free $LaNi_3$ compound. Formation of the monoclinically distorted $LaNi_3D_3$ deuteride proceeds via anomalously large anisotropic lattice expansion which is confined to the c-axis ($\Delta c/c$ = 30.6%). Selective filling by H atoms of the Laves type layers of $LaNi_3$ explains anomalously large expansion of these layers of 44−49% vol. % and was associated with a formation of the ···H···Ni···H···Ni··· chains with a covalent Ni−H bonding discovered by *ab initio* electronic structure calculations in $CeNi_3H_3$.[13,14]

The hydrogenation properties of the La_2MgNi_9 studied in the present work are dramatically different from those of $LaNi_3$, as a result of the replacement of 33% of La atoms by Mg. Indeed, in $La_2MgNi_9D_{13}$ hydrogen atoms are accommodated in both Laves and $CaCu_5$-type slabs, as shown in Figure 4. In the $LaNi_5$ $CaCu_5$-type layer, D atoms fill interstices with three types of metal environments: 2.36(4) at. D in deformed octahedron [La_2Ni_4] (D1 site), 2.27(6) at. D in [$La(Mg)_2Ni_2$] tetrahedra (D3 and D4 sites), and 0.56(2) at. D in [Ni_4] tetrahedron (D2 site) to yield $LaNi_5D_{5.2(1)}$ composition. Deuterium to metal ratio and D distribution are very similar to that in the deuteride of the individual $LaNi_5$ compound, β-$LaNi_5D_{5.9}$ (2.56 at. D in [La_2Ni_4], 2.77 at. D in [La_2Ni_2], and 0.57 at. D in [Ni_4]).[16]

In the Laves type layer of the $La_2MgNi_9D_{13}$ deuteride, $LaMgNi_4$, D atoms acquire four types of atomic coordination: trigonal bipyramidal [$(La/Mg)_3Ni_2$] for D5 site, tetrahedral [$(La/Mg)_2Ni_2$] for D6 site, tetrahedral [$(La/Mg)Ni_3$] for D7 site, and tetrahedral [Ni_4] for D8 site. Furthermore, common between $LaNi_5$ and $LaMgNi_4$ layers, tetrahedral [$(La/Mg)_2Ni_2$] sites are occupied by D3 and D4.

Triangular coordination [$(La/Mg)Ni_2$] of the D5 site is not typical for the Laves type hydrides and deserves special consideration. D5 is significantly shifted (by 0.6 Å) from the centers of two neighboring [$(La/Mg)_2Ni_2$] tetrahedra and occupies their common triangular face. Because of a mixed and statistical occupancy 50/50 by La and Mg of the 6*c* site, half of these triangular faces are [$LaNi_2$] and the other half are [$MgNi_2$]. Since the distance between La/Mg 6*c* and D5 sites is equal to 1.97(1) Å (atomic radii of La and Mg are 1.877 Å and 1.602 Å, respectively), the D5 site can only be filled in the case when it is coordinated by [$MgNi_2$] face and will be blocked for the accommodation of hydrogen atoms for the case of local [$LaNi_2$] coordination.

A similar situation characterizes local hydrogen ordering in the [$(La/Mg)_2Ni_2$] tetrahedra formed around the D6 site. Here one of the La/Mg−D6 distances is 2.03 Å and is too short for the large La atom. Thus, the D6 site may have coordination [$MgLaNi_2$] or [Mg_2Ni_2].

A list of interatomic distances between the occupied D sites and surrounding metal atoms is provided in Table S2 (Supporting Information). The minimum observed metal−hydrogen distances are 2.15(3) Å for La−D, 1.97(1) Å for Mg−D, and 1.52(1) Å for Ni−D.

In general, deuterium distribution in the structure of $La_2MgNi_9D_{13}$ can be rationalized by applying a geometric model[17] requiring a minimum radius of interstitial sites of 0.4 Å to accommodate hydrogen atoms and to form stable hydrides, and a minimum separation between H atoms of 2 Å to avoid strong repulsive interaction between them. These geometric criteria have been validated for many intermetallic Laves type and $CaCu_5$ type hydrides. In the $La_2MgNi_9D_{13}$ structure the filled interstices have radii exceeding 0.4 Å, in a range between 0.41 and 0.48 Å (see Table S2). Only for D5 [$MgNi_2$] and D8 [Ni_4] sites their radii, 0.37 and 0.39 Å, are slightly below the mentioned limiting value.

The 2 Å limit for the minimum H−H separations results in a partial and statistical occupancy of the hydrogen sites. None of the eight D sites in the structure of the deuteride appears to be completely filled: the maximum observed occupancy is for the D4 site, 58%; the occupancy of the other D sites is below 50%. Such low occupancies allow avoiding too short separations between the neighboring D sites below 2 Å (see Table S2). Repulsive H−H interactions prevent simultaneous filling of the neighboring D sites, leading to overall long-range disorder of D atoms in the structure.

A detailed analysis of the deuterium sublattice reveals some intriguing features, which cannot be explained solely on geometrical grounds. Figure 5 shows deuterium coordination of the metal atoms in the Laves type layers. Analysis shows that the mixed La/Mg position is surrounded by 22 partially occupied D sites: six of these sites are at distances of 2.0 Å, and 16 D-sites are located at 2.2−2.7 Å. Taking into account substantial size differences between atoms of Mg and La, it is reasonable to suggest that 16 larger Me−D distances, 2.2−2.7 Å, can be assigned to La. Thus, D atoms form a 16-vertex polyhedron around the La atom (only 12 vertices can be filled simultaneously to avoid the D···D blocking).

Naturally, the shortest distances (six in total per La/Mg site) correspond to the Mg−D ones. These six sites, if filled by the D

dx.doi.org/10.1021/ic202705u | *Inorg. Chem.* 2012, 51, 4231−4238

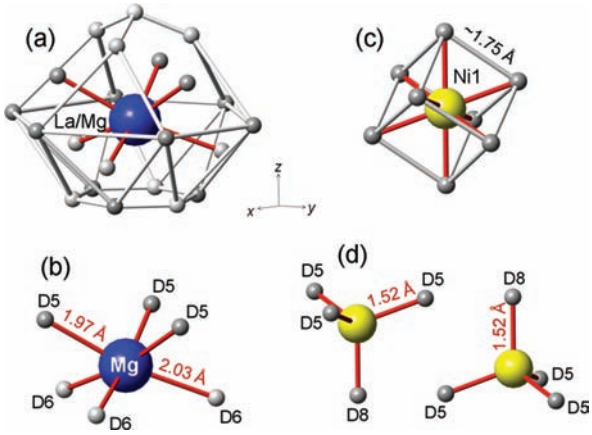

Figure 5. Local coordination of metal atoms by hydrogen in the Laves type slab of the $La_2MgNi_9D_{13}$ structure. (a) Two possible coordination spheres around mixed La/Mg position: external 16-vertex polyhedron corresponding to La atom, with metal–hydrogen distances in range 2.2–2.7 Å, and an internal deformed octahedron around Mg. (b) MgD_6 with much shorter Me–D distances of 2.0 Å. (c) Ni atom is coordinated by a cube of D sites of which only four can be occupied simultaneously as shown in part d. (d) Considering the limitations imposed by D···D blocking for interatomic distances less than 2 Å, local coordination of Ni atom can only be tetrahedron.

atoms, form a deformed octahedron around the Mg (Figure 5b). Similar MgD_6 octahedra were observed in the $LaMgNi_4$ layer of the hexagonal $La_3MgNi_{14}D_{18}$ deuteride,[6] and, more recently, in the structure of the cubic β-$CeMgCo_4D_4$.[18] Octahedral MgH_6 coordination appears to be typical for the saline type magnesium-based ternary hydrides[19] and binary MgH_2.[20] Indeed, the structures of both α- and γ-MgH_2 binary hydrides are built of MgD_6 octahedra, with Mg–D bond lengths 1.92–2.00 Å, which are in the same range as observed in the present system. This indicates that a local Mg–D bonding takes place in the $La_2MgNi_9D_{13}$. Calculations show that 4.5 H atoms from 7.9 H atoms in total in the $LaMgNi_4$ slab (nearly 60%) are directly bound to the Mg atoms.

Another very important feature of the structure of the $La_2MgNi_9D_{13}$ deuteride concerns local hydrogen ordering in the Ni–H coordination. Indeed, one of the nickel atoms, Ni1, has two types of the partially filled sites, D5 (six) and D8 (two), in its surrounding. Both D sites are half occupied. These sites form a cube $D5_6D8_2$ around Ni1 (Figure 5c), where rather short D–D edges of 1.73–1.77 Å prevent simultaneous occupation of all eight D vertexes. Assuming that D···D blocking fulfilling the "2 Å rule" is the case, two locally ordered NiD_4 units can be identified, with a minimum D–D distance of 2.5 Å in each of them. The $Ni1D5_3D8$ units form nearly ideal tetrahedra, with all Ni–D distances equal to 1.52(1) Å and D–Ni–D angles being in a close range between 108.6(3)° and 110.4(3)°. These latter values are very close to an ideal value of 109.5° for the regular tetrahedron. Two equivalent symmetry-related $Ni1D5_3D8$ tetrahedra are both oriented along [001], as shown in Figure 5d. The Ni–D distances of 1.52 Å in such tetrahedral units slightly exceed a sum of covalent radii of Ni and H, 1.47 Å,[21] and are within the range of the Ni–H distances of 1.50–1.60 Å reported for the Ni-containing complex hydrides.[22] Similar, even slightly shorter, values of the Ni–D bond lengths were observed in the chemically related La–Mg–Ni-based hydrides, $LaMg_2NiD_7$ (1.49 Å)[23] and $La_2MgNi_2D_8$ (1.50 Å).[24] The observed in $La_2MgNi_9D_{13}$ NiH_4 tetrahedra resemble the $(d^{10})sp^3$ $[NiH_4]^{4-}$, $[Ni_4H_{12}]^{12-}$, and $[Ni_2H_7]^{7-}$ hydrido complexes containing tetrahedral building blocks NiH_4 and observed in the Mg–Ni based complex hydrides, including Mg_2NiH_4,[25] $LaMg_2NiH_7$,[23] and $La_2MgNi_2H_8$.[24] On the other hand, the observed ordering is similar to known types of H–Ni ordering taking place in the structures of intermetallic hydrides, when a formation of the ···H···Ni···H···Ni··· chains in the $CeNi_3H_3$, $Ce_2Ni_7H_{4.7}$, and $LaNi_3H_3$ occurs. Thus, comparing these two mentioned for $La_2MgNi_9D_{13}$ options, the formation of the $[NiH_4]^{4-}$ hydrido complexes seems to be rather unlikely. The tetrahedral NiH_4 coordination apparently provides evidence for directional covalent Ni–H bonding, similar to those discovered by electronic structure calculations in $CeNi_3H_3$ and $Ce_2Ni_7H_{4.7}$.[14]

Analysis of the Ni–H coordination for the other two Ni atoms (Ni2 site in the $LaNi_5$ slab and Ni3 site at a boundary between $LaNi_5$ and Laves type slabs) in the structure of $La_2MgNi_9D_{13}$ showed presence of directional bonds between Ni and D atoms, 1.57–1.74 Å (see Supporting Information, Table S3). The observed Ni2–D and Ni3–D distances are noticeably longer than the Ni1–D ones thus indicating weaker Ni–H bonding, which nevertheless results in the formation of the locally ordered NiH_4 tetrahedra.

Obviously, on a long-range scale NiH_4 tetrahedra are disordered. Unfortunately, from the available crystallographic data it is not possible to conclude whether such tetrahedra form isolated units or are connected into the polynuclear frameworks in the structure.

A prominent and the most important feature of the structure of $La_2MgNi_9D_{13}$ is in local ordering of the hydrogen sublattice, which can be built by stacking of the MgH_6 octahedra and NiH_4 tetrahedra (see Figure 6). Every H vertex of the MgH_6 octahedron in such a sublattice is shared with two NiH_4 tetrahedra as shown in Figure 6a. However, a long-range order in stacking of the NiH_4 and MgH_6 polyhedra requires

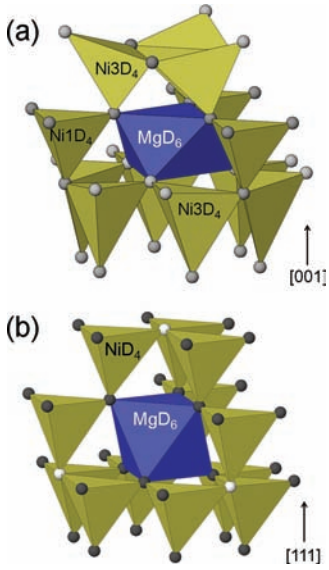

Figure 6. Hydrogen sublattice in the structures of the Mg–Ni-containing deuterides, (a) $La_2MgNi_9D_{13}$ and (b) γ-$LaMgNi_4D_7$. In both cases the sublattices are formed by stacking of the MgD_6 octahedra and NiD_4 tetrahedra. The stacking gives irregular, buckled ($La_2MgNi_9D_{13}$) or regular (γ-$LaMgNi_4D_7$) frameworks.

dx.doi.org/10.1021/ic202705u | Inorg. Chem. 2012, 51, 4231–4238

lowering of the crystal symmetry, which was not experimentally observed.

Interestingly, stacking of the octahedra MgH_6 and tetrahedra NiH_4 can also be observed in the structure of γ-$LaMgNi_4D_{4.85}$[15] formed on the basis of the $LaMgNi_4$ compound (ordered derivative of the cubic Laves phase structure with $MgCu_4Sn$ structure type) (see Figure 6b). In γ-$LaMgNi_4D_{4.85}$ D atoms form a regular MgD_6 octahedron around the Mg atoms (Mg−D distances equal to 2.01 Å) and a regular NiD_4 tetrahedron around the Ni atoms (with Ni−D distances of 1.58 Å). At the limiting composition $LaMgNi_4D_7$, the structure can be presented as a completely ordered spatial framework of the MgD_6 and NiD_4 polyhedra.

Comparison of the ordered hydrogen sublattices in $La_2MgNi_9D_{13}$ and in γ-$LaMgNi_4D_7$ shows that they are essentially the same and only slightly differentiated from each other because of the small buckling of the octahedra−tetrahedra network in $La_2MgNi_9D_{13}$ as compared to a precisely aligned similar network in γ-$LaMgNi_4D_7$.

It is clear that simple mechanisms of chemical bonding cannot be applied to describe the metal−hydrogen interactions in the $La_2MgNi_9H_{13}$ hydride. Indeed, the presently studied system is quite different from such quaternary hydrides as $LaMg_2NiH_7$[23,26] and $La_2MgNi_2H_8$,[24] where the hydrogenation of the initial intermetallics, $LaMg_2Ni$ and La_2MgNi_2, is accompanied by the metal−insulator transitions. This contrasts with the properties of $La_2MgNi_9H_{13}$ which is a good electronic conductor. Hydrogen distribution in both $LaMg_2NiH_7$ and $La_2MgNi_2H_8$ is completely ordered with full occupancy of all hydrogen positions, while the long-range H sublattice of $La_2MgNi_9D_{13}$ is disordered. Furthermore, in contrast with completely reversible hydrogen absorption and desorption by La_2MgNi_9, the hydride formation by $LaMg_2Ni$ and La_2MgNi_2 is irreversible, as their hydrides decompose into the binary lanthanum trihydride LaH_3 and amorphous constituents during the dehydrogenation.

In conclusion, La_2MgNi_9 has the highest hydrogen storage capacity among the characterized representatives of the hybrid La−Mg−Ni compounds relevant for applications in nickel−metal hydride batteries. Magnesium, when replacing lanthanum in the hybrid structure of La_2MgNi_9, introduces significant changes in the thermodynamic properties of the hydride and increases its stability against the hydrogen-induced disproportionation. Neutron diffraction studies of the saturated $La_2MgNi_9D_{13}$ hydride showed that H atoms favor occupation of Mg-surrounded sites within the $LaMgNi_4$ slabs, triangles $[MgNi_2]$, and tetrahedra $[LaMgNi_2]$; as a result, a local hydrogen ordering takes place with the hydrogen sublattice built from a stacking of the MgH_6 octahedra and NiH_4 tetrahedra. These conclusions are supported by a good agreement between the partial 50/50 La2/Mg occupancy, filling of the hydrogen sites, and hydrogen ordering around the Ni atoms. The $La_2MgNi_9D_{13}$ deuteride forms a link between complex and interstitial hydrides, representing structural features typical for both types of hydrides. Electronic structure calculations will be useful to shed light on the nature of the metal−hydrogen bonding in the $La_{3-x}Mg_xNi_9$-based hydrides.

■ ASSOCIATED CONTENT

Supporting Information

Tables and figures giving details of crystallographic analysis of $La_2MgNi_9D_{13}$; crystal data in CIF format. This material is available free of charge via the Internet at http://pubs.acs.org.

■ AUTHOR INFORMATION

Corresponding Author

*E-mail: volodymyr.yartys@ife.no.

Notes

The authors declare no competing financial interest.

■ ACKNOWLEDGMENTS

This work has received a support from the program NANOMAT of Norwegian Research Council (Project 203323). The authors are grateful to the staff of the Swiss-Norwegian Beamlines, Grenoble, France, for the skillful assistance during the SR XRD experiments. The neutron diffraction experiments were performed at the Swiss Spallation Neutron Source, Paul Scherrer Institute, Villigen, Switzerland (Experiment 20101348). We are grateful to Dr. Denis V. Sheptyakov (Laboratory for Neutron Scattering, PSI) for the help during the work at PSI.

■ REFERENCES

(1) Kohno, T.; Yoshida, H.; Kawashima, F.; Inaba, T.; Sakai, I.; Yamamoto, M.; Kanda, M. *J. Alloys Compd.* **2000**, *311*, L5−L7.

(2) Ozaki, T.; Kanemoto, M.; Kakeya, T.; Kitano, Y.; Kuzuhara, M.; Watada, M.; Tanase, S.; Sakai, T. *J. Alloys Compd.* **2007**, *446*−*447*, 620−624.

(3) Hayakawa, H.; Akiba, E.; Gotoh, M; Kohno, T. *Mater. Trans.* **2005**, *46* (6), 1393−1401.

(4) Férey, A.; Cuevas, F.; Latroche, M.; Knosp, B.; Bernard, P. *Electrochim. Acta* **2009**, *54*, 1710−1714.

(5) Zhang, Q.; Fang, M.; Si, T.; Fang, F.; Sun, D.; Ouyang, L.; Zhu, M. *J. Phys. Chem. C* **2010**, *114*, 11686−11692.

(6) Denys, R. V.; Riabov, A. B.; Yartys, V. A.; Sato, M.; Delaplane, R. G. *J. Solid State Chem.* **2008**, *181*, 812−821.

(7) Yartys, V. A.; Riabov, A. B.; Denys, R. V.; Sato, M.; Delaplane, R. G. *J. Alloys Compd.* **2006**, *408*−*412*, 273−279.

(8) Nakamura, J.; Iwase, K.; Hayakawa, H.; Nakamura, Y.; Akiba, E. *J. Phys. Chem. C* **2009**, *113*, 5853−5859.

(9) Denys, R. V.; Yartys, V. A. *J. Alloys Compd.* **2011**, *509* (Supplement 2), S540−S548.

(10) Liao, B.; Lei, Y. Q.; Lu, G. L.; Chen, L. X.; Pan, H. G.; Wang, Q. D. *J. Power Sources* **2004**, *129*, 358−367.

(11) Rodriguez-Carvajal, J. *Physica B* **1993**, *192*, 55−69.

(12) Toby, B. H. *J. Appl. Crystallogr.* **2001**, *34*, 210−213.

(13) Denys, R. V.; Riabov, A. B.; Yartys, V. A.; Delaplane, R. G.; Sato, M. *J. Alloys Compd.* **2007**, *446*−*447*, 166−172.

(14) Yartys, V. A.; Vajeeston, P.; Riabov, A. B.; Ravindran, P.; Denys, R. V.; Maehlen, J. P.; Delaplane, R. G.; Fjellvåg, H. *Z. Kristallogr.* **2008**, *223*, 674−689.

(15) Chotard, J.-N.; Sheptyakov, D.; Yvon, K. *Z. Kristallogr.* **2008**, *223*, 690−696.

(16) Lartigue, C.; Percheron-Guégan, A.; Achard, J. C.; Soubeyroux, J. L. *J. Less-Common Met.* **1985**, *113*, 127−148.

(17) Westlake, D. G. *J. Less-Common Met.* **1983**, *90*, 251−273.

(18) Denys, R. V.; Riabov, A. B.; Černý, R.; Koval'chuk, I. V.; Zavaliy, I. Yu. *J. Solid State Chem.* **2012**, *187*, 1−6.

(19) Yvon, K.; Bertheville, B. *J. Alloys Compd.* **2006**, *425*, 101−108.

(20) Bortz, M.; Bertheville, B.; Bottger, G.; Yvon, K. *J. Alloys Compd.* **1999**, *287*, L4−L6.

(21) Yvon, K.; Fischer, P. In *Hydrogen in Intermetallic Compounds I*; Schlapbach, L., Ed.; Topics in Applied Physics; Springer: Berlin, 1988; Vol. *63*, p 109.

(22) Yvon, K.; Renaudin, G. Hydrides: Solid State Transition Metal Complexes. *Encyclopedia of Inorganic Chemistry*, 2nd ed.; King, R. B., Ed.; John Wiley & Sons, Ltd: Chichester, U.K., 2005; Vol. 3, pp 1814−1846.

(23) Renaudin, G.; Guénée, L.; Yvon, K. *J. Alloys Compd.* **2003**, *350*, 145−150.

(24) Chotard, J.-N.; Filinchuk, Y.; Revaz, B.; Yvon, K. *Angew. Chem., Int. Ed.* **2006**, *45*, 7770−7773.
(25) Zolliker, P.; Yvon, K.; Jorgensen, J. D.; Rotella, F. J. *Inorg. Chem.* **1986**, *25*, 3590−3593.
(26) Yvon, K.; Renaudin, G.; Wei, C. M.; Chou, M. Y. *Phys. Rev. Lett.* **2005**, *94*, 066403−1−4.